

Document made available under the Patent Cooperation Treaty (PCT)

International application number: PCT/US2008/000791

International filing date: 22 January 2008 (22.01.2008)

Document type: Certified copy of priority document

Document details: Country/Office: US
Number: 60/881,837
Filing date: 23 January 2007 (23.01.2007)

Date of receipt at the International Bureau: 20 March 2008 (20.03.2008)

Remark: Priority document submitted or transmitted to the International Bureau in compliance with Rule 17.1(a) or (b)



51168

THE UNITED STATES OF AMERICA

TO ALL TO WHOM THESE PRESENTS SHALL COME:

UNITED STATES DEPARTMENT OF COMMERCE

United States Patent and Trademark Office

March 20, 2008

THIS IS TO CERTIFY THAT ANNEXED HERETO IS A TRUE COPY FROM THE RECORDS OF THE UNITED STATES PATENT AND TRADEMARK OFFICE OF THOSE PAPERS OF THE BELOW IDENTIFIED PATENT APPLICATION THAT MET THE REQUIREMENTS TO BE GRANTED A FILING DATE.

APPLICATION NUMBER: *60/881,837*

FILING DATE: *January 23, 2007*

RELATED PCT APPLICATION NUMBER: *PCT/US08/00791*

THE COUNTRY CODE AND NUMBER OF YOUR PRIORITY APPLICATION, TO BE USED FOR FILING ABROAD UNDER THE PARIS CONVENTION, IS *US60/881,837*



Certified by

A handwritten signature in black ink, appearing to read "Jon W. Dudas".

Under Secretary of Commerce
for Intellectual Property
and Director of the United States
Patent and Trademark Office

PTO/SB/16 (07-06)

Approved for use through 01/31/2007. OMB 0651-0032

U.S. Patent and Trademark Office; U.S. DEPARTMENT OF COMMERCE

Under the Paperwork Reduction Act of 1995, no persons are required to respond to a collection of information unless it displays a valid OMB control number.

PROVISIONAL APPLICATION FOR PATENT COVER SHEET - Page 1 of 2

This is a request for filing a PROVISIONAL APPLICATION FOR PATENT under 37 CFR 1.53(c).

Express Mail Label No. _____

17712 U.S. PTO
012307

INVENTOR(S)		
Given Name (first and middle [if any])	Family Name or Surname	Residence (City and either State or Foreign Country)
GHASSAN S.	KASSAB	ZIONSVILLE, IN
THOMAS	WISCHGOLL	DAYTON, OH
Additional inventors are being named on the _____ separately numbered sheets attached hereto		
TITLE OF THE INVENTION (500 characters max):		
IMAGE-BASED EXTRACTION FOR VASCULAR TREES		
Direct all correspondence to: CORRESPONDENCE ADDRESS		
<input checked="" type="checkbox"/> The address corresponding to Customer Number: 39,013		
OR		
<input type="checkbox"/> Firm or Individual Name		
Address		
City	State	Zip
Country	Telephone	Email
ENCLOSED APPLICATION PARTS (check all that apply)		
<input type="checkbox"/> Application Data Sheet. See 37 CFR 1.76 <input type="checkbox"/> CD(s), Number of CDs _____		
<input checked="" type="checkbox"/> Drawing(s) Number of Sheets <u>7</u> <input checked="" type="checkbox"/> Other (specify) <u>PTO-2038 credit card auth. form</u>		
<input checked="" type="checkbox"/> Specification (e.g. description of the invention) Number of Pages <u>28</u>		
Fees Due: Filing Fee of \$200 (\$100 for small entity). If the specification and drawings exceed 100 sheets of paper, an application size fee is also due, which is \$250 (\$125 for small entity) for each additional 50 sheets or fraction thereof. See 35 U.S.C. 41(a)(1)(G) and 37 CFR 1.16(s).		
METHOD OF PAYMENT OF THE FILING FEE AND APPLICATION SIZE FEE FOR THIS PROVISIONAL APPLICATION FOR PATENT		
<input checked="" type="checkbox"/> Applicant claims small entity status. See 37 CFR 1.27. 100		
<input type="checkbox"/> A check or money order is enclosed to cover the filing fee and application size fee (if applicable).		
<input checked="" type="checkbox"/> Payment by credit card. Form PTO-2038 is attached TOTAL FEE AMOUNT (\$)		
<input checked="" type="checkbox"/> The Director is hereby authorized to charge the filing fee and application size fee (if applicable) or credit any overpayment to Deposit TOTAL FEE AMOUNT (\$)		
Account Number: <u>502882</u> A duplicative copy of this form is enclosed for fee processing.		

USE ONLY FOR FILING A PROVISIONAL APPLICATION FOR PATENT

This collection of information is required by 37 CFR 1.51. The information is required to obtain or retain a benefit by the public which is to file (and by the USPTO to process) an application. Confidentiality is governed by 35 U.S.C. 122 and 37 CFR 1.11 and 1.14. This collection is estimated to take 8 hours to complete, including gathering, preparing, and submitting the completed application form to the USPTO. Time will vary depending upon the individual case. Any comments on the amount of time you require to complete this form and/or suggestions for reducing this burden, should be sent to the Chief Information Officer, U.S. Patent and Trademark Office, U.S. Department of Commerce, P.O. Box 1450, Alexandria, VA 22313-1450. DO NOT SEND FEES OR COMPLETED FORMS TO THIS ADDRESS. **SEND TO: Commissioner for Patents, P.O. Box 1450, Alexandria, VA 22313-1450.**

If you need assistance in completing the form, call 1-800-PTO-9199 and select option 2.

PROVISIONAL APPLICATION COVER SHEET
Page 2 of 2

PTO/SB/16 (07-08)

Approved for use through 01/31/2007. OMB 0651-0032

U.S. Patent and Trademark Office: U.S. DEPARTMENT OF COMMERCE

Under the Paperwork Reduction Act of 1995, no persons are required to respond to a collection of information unless it displays a valid OMB control number.

The invention was made by an agency of the United States Government or under a contract with an agency of the United States Government.



No.

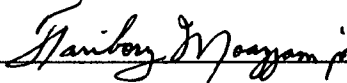


Yes, the name of the U.S. Government agency and the Government contract number are: _____

WARNING:

Petitioner/applicant is cautioned to avoid submitting personal information in documents filed in a patent application that may contribute to identity theft. Personal information such as social security numbers, bank account numbers, or credit card numbers (other than a check or credit card authorization form PTO-2038 submitted for payment purposes) is never required by the USPTO to support a petition or an application. If this type of personal information is included in documents submitted to the USPTO, petitioners/applicants should consider redacting such personal information from the documents before submitting them to the USPTO. Petitioner/applicant is advised that the record of a patent application is available to the public after publication of the application (unless a non-publication request in compliance with 37 CFR 1.213(a) is made in the application) or issuance of a patent. Furthermore, the record from an abandoned application may also be available to the public if the application is referenced in a published application or an issued patent (see 37 CFR 1.14). Checks and credit card authorization forms PTO-2038 submitted for payment purposes are not retained in the application file and therefore are not publicly available.

SIGNATURE _____



Date 23 JANUARY 2007

TYPED or PRINTED NAME FARIBORZ MOAZZAM

REGISTRATION NO. 53,339
(if appropriate)

TELEPHONE 703-442-9480

Docket Number: KAS-134-PRO

**PROVISIONAL
APPLICATION FOR UNITED STATES LETTERS PATENT**

by

**GHASSAN S. KASSAB
THOMAS WISCHGOLL**

for

IMAGE-BASED EXTRACTION FOR VASCULAR TREES

**MOAZZAM & ASSOCIATES, LLC
7601 Lewinsville Road, Suite 304
McLean, VA 22102
(703) 442-9480**

Attorney Docket No.: KAS-134-PRO

IMAGE-BASED EXTRACTION FOR VASCULAR TREES

BACKGROUND OF THE INVENTION

Field of the Invention

[0001] The present invention relates generally to medical imaging. More particularly, the present invention relates to mapping the vascular system.

Background of the Invention

[0002] The analysis of spatial perfusion of any organ requires detailed morphometry on the geometry (diameters, lengths, number of vessels, etc.) and branching pattern (3-D angles, connectivity of vessels, etc.). Despite the significance of morphometric data for understanding spatial distribution of blood flow and hemodynamics, the data are relatively sparse. One of the major reasons for the scarcity of morphometric data is the tremendous labor involved. To reconstruct and count a significant number of vessels in most organs is an extremely labor-intensive endeavor. What is needed is the development of labor-saving methodology.

[0003] Several approaches for extracting curve-skeletons or medial axis can be found in the literature. Different studies can be found on segmentation of volumetric data sets. The approaches include surface extraction based on an energy function using the image gradient; deformable meshes; hysteresis thresholding and region growing; m-reps, skeletons composed of atoms (hubs) connected to the surface; and distance to the vessel wall combined with a penalty function. To improve the segmentation, Lei et al. deployed fuzzy

connectedness to segment vessels and distinguish between arteries and veins while Chung et al. used different mixture models. Gan et al. analyzed the maximum intensity distribution to identify optimal thresholds to extract vessels from a series of maximum intensity projections. By using an atlas, Passat et al. divided the human brain into different areas to identify more suitable thresholds for each of these areas to optimize a region growing segmentation of brain vessels. Subsequently, the atlas was refined by adding morphological data, such as vessel diameter and vessel orientation, to extract a vascular tree from phase contrast MRA data. Centerlines extracted using the algorithm by Aylward et al. based on intensity ridge traversal were smoothed using a B-spline-based approach to get smoother results. Zhang et al. described a centerline extraction algorithm based on Dijkstra's algorithm using a distance-field cost function. The jagged lines that typically result from voxel-based centerline extraction algorithms were smoothed using either cubic splines or Chebyshev polynomials. Other artifacts from the results of a 3-D thinning algorithm, such as cycles, spurs, and non-unit-width parts, can be removed by using an approach by Chen et al. Ukil et al. introduced a smoothing approach for airways of a lung based on an ellipsoidal kernel before segmenting and thinning the 3-D volumetric image.

[0004]

To describe a geometric model of the vessels of brain data sets, Volkau et al. used the centerline and radii to describe cylinders. The centerlines were smoothed using average filtering to avoid self-intersections of the cylinders. The surfaces of the cylinders were modeled following a Catmull-Clark sub-division surface approach. For extracting centerlines from volumetric images, topology-

connectivity-preserving thinning is a common approach. By using the Hessian of the image intensity, Bullet et al. developed a ridge line detection method to identify centerlines. Once the centerline is determined, quantitative data, such as lengths, areas, and angles, can be extracted as shown by Martinenez-Perez et al. and Wan et al. A detailed data structure for building an airway tree was described by Chaturvedi et al. Recently, Nordsletten et al. proposed an approach that segments vessels of a rat's kidney based on iso-surface computation. Using the surface normals, the surface was projected to the center of the vessels, while a snake algorithm collects and connects the resulting point cloud. To analyze the branching morphology of the rat hepatic portal vein tree, Den Buijs et al. compared the radii and branching angles of the vessels to a theoretical model of dichotomous branching.

[0005] Software-based analysis and computation of the vector field of a vascular tree has been slow and cumbersome. Some methods begin with all voxels of a volumetric image and use a thinning technique to shrink down the object to a single line. Directional thinning approaches use a specific order in which voxels are removed. For example, directions, such as up or down, are used to define this order and conditions are used to identify endpoints. Since these methods are sensitive with respect to the order in which the voxels are removed, the resulting curve-skeleton may not be centered. Non-directional methods or fully parallel approaches do not have this disadvantage. Ideally, the topology of the object should be observed. Such an approach was proposed by Lobregt et al. which is the basic technique used in commercial software systems, such as Analyze™.

The disadvantage of this approach is that it tends to produce jagged lines which do not allow accurate measurements of angles between parts of the object, such as individual segments of a vascular structure. Other approaches classify the voxels in different groups, such as edge, inner, curve, or junction and are re-classified after removal of a voxel. A similar algorithm is proposed by Palagyi et al. The disadvantage of thinning algorithms is that they can only be applied to volumetric data sets. Since the approach presented in this paper is not based on voxels it can be applied to non-volumetric data; i.e., it is also applicable to geometric data sets. Furthermore, the location of the centerline is determined at a higher numerical precision since its defining points are not bound to a single voxel. This also helps avoid the jagged representation of the centerlines.

[0006]

Other approaches use the distance transform or distance field in order to obtain a curve-skeleton. For each point inside the object, the smallest distance to the boundary surface is determined. For this, the Euclidian metric or the $\langle 3,4,5 \rangle$ metric can be used. Also, fast marching methods can be deployed to compute the distance field. Voxels representing the centerlines of the object are identified by finding ridges in the distance field. The resulting candidates must then be pruned first. The resulting values are connected using a path connection or minimum span tree algorithm. Methods used to identify points on the ridges include distance thinning, divergence computing, gradient searching, thresholding the bisector angle, geodesic front propagation, or shrinking the surface along the gradient of the distance field. The distance field can also be combined with a distance-from-source field to compute a skeleton. Similar to

thinning approaches, these methods are voxel-based and tend to generate the same jagged centerlines. This implies that a centerline can deviate from its original location by up to half a voxel due to the numerical representation. The proposed approach does not suffer from this problem as it uses a higher numerical precision for computing the centerlines.

[0007] A more recent method by Cornea et al. computes the distance field based on a potential similar to an electrical charge and then uses a 3D topological analysis to determine the centerlines. This approach, however, suffers from a few disadvantages when applied to CT scanned volumetric images. For example, computing the distance field alone would take several months. Furthermore, due to the rare occurrence of 3D singularities used as starting point for topological analysis, additional criteria have to be imposed. The method presented in this paper avoids this by linearly interpolating the vector field within the vessels and performing a 2-D topological analysis in cross sections of the vessels only. This results in a significantly shorter computational time for generation of data which is very important for large data sets in larger species.

[0008] Techniques based on Voronoi diagrams define a medial axis using the Voronoi points. Since this approach usually does not result in a single line but rather a surface shaped object, the points need to be clustered and connected in order to obtain a curve-skeleton. Voronoi-based methods can be applied to volumetric images as well as point sets. Due to the fact that clustering of the resulting points is required, these approaches lack accuracy. In addition, they tend to create points outside the object itself if there is an open or missing area

within the object's boundary.

[0009] For extracting centerlines from volumetric images, geometry-based approaches are more preferable over voxel-based approaches. Due to the discrete nature of a voxel of the volumetric image, the location of the centerline can be off by half a voxel. Geometry-based methods do not suffer from this problem. Nordsletten et al. compute normal vectors based on an iso-surface computed using the volumetric image. These normal vectors are then projected inwards. The resulting point cloud is then collected and connected by a snake algorithm. Since this method estimates the normal vectors, the center of the vessel is not necessarily in the direction of the normal vector. Hence, the computed centerline may not be accurate. Using vector field topology analysis, the proposed technique compensates for this automatically. It is therefore expected that a more precise computation of center points is possible. The approach based on a 3-D vector field analysis proposed by Cornea et al. results in a very accurate computation of the centerlines. The only difficulty with this approach is that computing the centerlines for a CT scanned volumetric image of the size 512 by 512 by 200 would take several months, which renders it inapplicable in this case.

[0010] What is needed is a technique for extracting vascular structures from volumetric images that does not suffer from some of the drawbacks of conventional methods, is efficient and easy to use, intuitive and based on more physiological conditions than prior techniques.

SUMMARY OF THE INVENTION

[0011] The present invention is capable of extracting vascular structures from volumetric images and computing the diameters of the vessels in a more efficient manner. The validation of the computed diameters by comparing the computed values with manually measured diameters shows the accuracy of the method. The method itself is not only capable of extracting the main trunk, but also the entire vascular tree. Hence, the approach allows the extraction of accurate quantitative data for the entire vasculature.

[0012] In one exemplary embodiment, the present invention is a computer program product that utilizes a less computationally intensive way of computing the vector field. Also, the topological analysis of the 2-D vector fields within cross-sectional areas of the vessels can be computed more efficiently. This allows the processing of a CT scanned data set within a few hours which potentially can be reduced by optimization of the code making it more efficient. In addition to requiring less computational time, the proposed algorithm does not require the introduction of artificial starting points for the topological analysis. As a matter of fact, the singularities defining the centerlines are generated by projecting the vector field onto the cross-sectional areas of the vessels.

[0013] In another embodiment, the software will be used to extract the entire vascular tree from the CT-scanned volumetric images. This will allow the determination of vessel diameters and lengths as well as bifurcation angles within the vasculature. Such accurate and detailed anatomical models will then serve as an architectural platform for hemodynamic analysis of blood flow.

BRIEF DESCRIPTION OF THE DRAWINGS

- [0014]** FIG. 1 shows a flow chart outlining basic steps of the algorithm, according to an exemplary embodiment of the present invention.
- [0015]** FIGS. 2A, B, C show a direct comparison for typical specimens between manually measured and computed diameters for the LAD, LCX, and the RCA trunks respectively, according to an exemplary embodiment of the present invention.
- [0016]** FIGS. 3A, B, C shows a comparison between the manually measured and computed diameters for a series of specimens with respect to the LAD trunk, LCX artery, and RCA, according to an exemplary embodiment of the present invention.
- [0017]** FIGS. 4 A-F respectively show saddle, node, focus, center, spiral, and improper node singularities of a vector field including surrounding flow, according to an exemplary embodiment of the present invention.
- [0018]** FIG. 5A shows determination of the sub-voxel precision of a voxel and its neighboring voxels, while FIG. 5B shows computation of the local maximum for the gradient, according to an exemplary embodiment of the present invention.
- [0019]** FIG. 6 shows a volume rendering of a Microfil perfused porcine heart scanned using a CT scanner.
- [0020]** FIG. 7 shows a curve-skeleton of the porcine heart data set according to an exemplary embodiment of the present invention.
- [0021]** FIG. 8A and B show a sub-section of the porcine heart data set visualized

as a volume rendered image and as an extracted curve-skeleton respectively, according to an exemplary embodiment of the present invention.

DETAILED DESCRIPTION OF THE INVENTION

[0022] The present invention is a method for extracting vessels from a CT image of porcine coronary arteries. This method identifies the vessels and determines the centerlines of those vessels; i.e., it reduces the entire vasculature to a stick-like curve-skeleton. In one embodiment, the present invention is a computer program product that computes the vessel diameter at any given point as the distance between the centerline and the vessel wall, as well as the angles between vessels. Furthermore, the method is validated against manually determined optical measurements of vessel diameters to assess its accuracy.

[0023] Methods:

[0024] *CT Images of Coronary Arteries:* Five hearts from normal Yorkshire swine of either sex with body weight of 34.3- 42.1 kg were studied. The animals were fasted overnight; Ketamine, 20 mg/kg, and atropine, 0.05 mg/kg, were administered intramuscularly before endotracheal intubation. The animals were ventilated using a mechanical respirator and general anesthesia was maintained with 1-2% isoflurane and oxygen. The chest was opened through a midsternal thoracotomy, and an incision was made in the pericardium to reach the heart. The animals were then deeply anesthetized followed by an injection of a saturated KCl solution through the jugular vein to arrest the heart. The aorta was clamped to keep air bubbles from entering the coronary arteries, and the heart

was excised and placed in a saline solution. The LAD artery, the right coronary artery (RCA) and the left circumflex (LCX) artery were cannulated under saline to avoid air bubbles and perfused with cardioplegic solution to flush out the blood. The three major arteries (RCA, LAD and LCX) were individually perfused at a pressure of 100 mmHg with three different colors of Microfil (Flow Tech Inc.). After the Microfil was allowed to harden for 45 to 60 minutes the hearts were kept in the refrigerator in saline solution until the day the CT scan was performed. The scans were made axially (120mas 120kv, 0.6/0.6mm slice) on a 16 slice scanner (Siemens Somatom)

[0025] *Optical Measurements of Vessel Trunk:* After the CT scan was performed, the cast hearts were immersed and macerated in 30% potassium hydroxide solution for 3 to 4 days to remove the tissue and obtain a cast of the coronary arteries and their branches. The trunk of the LAD, RCA and LCX casts were then photographed using a dissection microscope and a color digital camera (Nikon). For each photograph the diameter of the three main trunks were measured at each branch from the proximal artery to where the trunk becomes < 1 mm in diameter. The optical measurements were made using SigmaScan Pro 5 software. The measurements were then compared to the values retrieved from the extraction algorithm.

[0026] *Computer-Assisted Extraction of Morphometric Data from CT Volumetric Images:* The present invention proposes to extract morphometric data from a volumetric image in several steps. **FIG. 1** outlines the basic steps. The algorithm first segments the vessels within the volumetric image based on the image

gradients. In order to get a more accurate representation of the vessel boundary, the points resulting from the segmentation step are moved along the gradient direction in such a way that they are located at the maximal gradient. This provides a more precise and smoother representation of the boundary. Then, a vector field is computed in such a way that all vectors are pointing inwards to the center of the vessel. In the simplest case, the image gradients can be used at the boundary. Using a tri-linear interpolation, the vector field can be computed after a tetrahedrization of all the boundary points is determined. Finally, the points on the centerlines are computed using a topological analysis of the vector field within the cross sectional area of the vessels and connected based on the topology of the tetrahedrization. This then results in a precise representation of the centerlines of all vessels within the volumetric image. The major trunk defined along the larger diameter at each bifurcation was determined and compared to the manual optical measurements.

[0027] *Data and Statistical Analysis:* The position along the RCA, LAD and LCX arteries was normalized with respect to the total length (from inlet of artery down to 1 mm diameter). Hence, the results were expressed in terms of fractional longitudinal position (FLP), ranging from 0 to 1. The data for both the independent (FLP) and dependent variables (diameter) were then divided into 20 equal intervals: 0-0.05, 0.06-0.1, 0.11-0.15 ... 0.9-0.95, 0.96-1.0. The results were expressed as means \pm 1SD over each interval. A t-test was used to detect possible differences between groups and intervals.

[0028] Results:

[0029] In order to validate the results derived from CT imaging software, the manual optical measurements were compared to the computed values for the main trunks of the LAD, LCX, and the RCA branches. **FIG. 2A** shows a typical example of the LAD trunk for one representative heart. As can be seen from the two curves, the diameters that were manually measured (dashed) agree with the ones determined by the software system (solid) very well. **FIGS. 2B** and **C** show the results for the LCX and RCA branch of the same heart, respectively. There was no statistically significant difference between the two measurements ($p>0.05$).

[0030] In order to facilitate a direct comparison between the manually measured data and the computed values, the data were normalized along the length to a scale between zero and one. The most proximal artery was identified as zero, while the vessel of 1mm diameter was set to one. Figures 3A-C show the comparison of the manually measured and computer-based diameters. The vertical bars represent the standard deviation within each bin. Similarly, the range of values within each bin is demonstrated. As can be seen from these graphs, the manually measured diameters agree very well with the computer-generated values. There were no statistically significant differences between the two sets of measurements at each interval ($p>0.05$). Furthermore, the root mean square error between the two measurements of all vessels is 0.16 mm (0.21 mm for LAD, 0.14 mm for LCX, and 0.11 mm for RCA) which is < 10% of the mean value.

[0031] Computer-Assisted Extraction of Morphometric Data from CT Volumetric Images:

[0032] Before illustrating the algorithm used to extract quantitative information from the CT scanned volumetric images, the theoretical foundation of the methodology will be outlined. Hence, the next sections briefly summarize the main ideas of 2-D vector field topology.

[0033] *Topological Analysis of Vector Fields:* The algorithm described in this paper uses the topology of a vector field defined on the faces of a tetrahedralized set of points. Thus, the vector field is defined by three vectors located at the vertices of a triangle. The vector field in between the triangles is interpolated linearly by computing the barycentric coordinates of the point within the triangle. These coordinates are then used as weights for linearly combining the three vectors defined at the vertices of the triangle to compute the interpolated vector. The advantage of such a linear interpolation is an easier classification of topological features as described in the following subsections.

[0034] *Critical Points:* Critical points are an important feature from a topological point of view since they are used as starting points for the topological analysis. Let v be a given vector field $v:W \rightarrow R^3$ with $W \subset R^3$ as defined on a face of a tetrahedron. Let further $x_0 \in W$ be a point where the vector field vanishes, i.e. $v(x_0) = 0$. Then x_0 is considered a critical point of the vector field v . Several terms are used synonymously for critical points. These are singularities, singular points, zeros, or equilibrium. Due to the fact that linear interpolation is used to interpolate across a face of a tetrahedron; i.e., a triangle, the vector field v can be described in this case by a matrix and a displacement vector. Therefore, a linear map $A:W \rightarrow R^3$ described by the 3×3 matrix A and a vector $b \in R^3$ can be found such

that it describes the given vector field v (i.e., $v(x) = Ax + b$ for all $x \in W$). Then, singularities can be identified by directly solving the equation $Ax + b = 0$.

Obviously, there cannot be more than one singularity located within one triangle when using linear interpolation. For the case $b = 0$ we consider the vector field described by Ax homogenous linear. Without loss of generality we assume homogenous linear vector fields in the further discussion of the theory of vector field topology throughout this section of the paper.

[0035] Singularities can be classified using the eigenvalues of the interpolating matrix A regarding their property of attracting or repelling the surrounding flow. If all eigenvalues have negative real parts, the singularity is considered a sink which attracts the surrounding flow. On the other hand, if all eigenvalues have positive real parts the singularity is a source that repels the surrounding flow. A proof for this classification can be found in the book of Hirsch and Smale. Further analysis of matrix A leads to several types of vector fields distinguished by their major properties of the flow; i.e., the behavior of the streamlines within this vector field. In order to compute a streamline, the Cauchy problem has to be solved with initial problem $x(0) = k, k \in \mathbb{R}^3$:

[0036]
$$\frac{d}{dt} x(t) = Ax(t) \tag{1}$$

[0037] It can be easily proven that the solution to the Cauchy problem for a linear vector field can be described by an exponential function:

[0038]
$$x = e^{tA} k \quad \text{with} \quad e^A = \sum_{i=0}^{\infty} \frac{A^i}{i!} \tag{2}$$

[0039] Different categories of vector fields can then be distinguished based on

whether the matrix A is diagonalizable. This leads to three main categories which are described below.

[0040] *Linear Vector Fields of Type 1* - The matrix A is diagonalizable; i.e., the eigenvalues λ and μ are real. Thus it is similar to a matrix B where there exists an invertible matrix P with $B = PAP^{-1}$, of the following structure:

$$B = \begin{pmatrix} \lambda & 0 \\ 0 & \mu \end{pmatrix} \quad (3)$$

[0041]

[0042] Due to the structure of the matrix B , a streamline $x(t)$ with initial condition $k = (k_1, k_2)$ can be computed in a vector field described by such a matrix using the following formula:

$$x(t) = \begin{pmatrix} e^{\lambda t} k_1 \\ e^{\mu t} k_2 \end{pmatrix} \quad (4)$$

[0043]

[0044] By computing streamlines we generate a phase portrait of the different cases of vector fields within this category. Three different types are possible as distinguished by the eigenvalues of the interpolating matrix A . The first case, where $\lambda > 0 > \mu$, results in a saddle singularity. An example is depicted in Fig 4A. The second case, described by an eigenvalue configuration of $\lambda < \mu < 0$, describes a node singularity as shown in Fig 4B. The last case with two identical eigenvalues is the focus singularity. Fig 4C shows a focus singularity with $\lambda = \mu < 0$. The examples shown here are mainly of sinks. The same types of singularities occur, however, with sources. The only difference is in the sign of the eigenvalues; i.e., multiplying the eigenvalues by -1 results in the same singularities as sources by simply reversing the flow.

[0045] *Linear Vector Fields of Type 2* - The two eigenvalues of the matrix A have a non-imaginary part; i.e., A is similar to the following matrix:

$$B = \begin{pmatrix} a & -b \\ b & a \end{pmatrix} \quad (5)$$

[0047] When substituting the values a and b in the above matrix by introducing new values θ and r , namely,

$$\begin{aligned} r &= \sqrt{a^2 + b^2} \\ \theta &= \arccos(a/r) \end{aligned} \quad (6)$$

[0049] the matrix B can be rewritten as follows:

$$B = \begin{pmatrix} a & -b \\ b & a \end{pmatrix} = \begin{pmatrix} r & 0 \\ 0 & r \end{pmatrix} \cdot \begin{pmatrix} \cos \theta & -\sin \theta \\ \sin \theta & \cos \theta \end{pmatrix} \quad (7)$$

[0051] Obviously, a vector field described by such a matrix has a strong rotational component. Consequently, a streamline $x(t)$ with initial condition $k = (k_1, k_2)$ can be computed using the following formula (45):

$$x(t) = e^{ta} \cdot \begin{pmatrix} k_1 \cos(tb) - k_2 \sin(tb) \\ k_1 \sin(tb) + k_2 \cos(tb) \end{pmatrix} \quad (8)$$

[0053] A center singularity results if $a = 0$ which is described by a phase portrait that consists of streamlines forming concentric circles with the singularity as their center. An example is shown in Fig 4D. Otherwise, a spiral singularity is described with streamlines spiraling around the singularity and then eventually ending up at the singularity itself as shown in Fig 4E.

[0054] *Linear Vector Fields of Type 3* - If the matrix A is not diagonalizable and the two eigenvalues are equal ($\lambda = \mu$) then A is similar to the following matrix:

[0055]
$$B = \begin{pmatrix} \lambda & 0 \\ 1 & \lambda \end{pmatrix} \quad (9)$$

[0056] By splitting up the matrix B into two components, we obtain:

[0057]
$$B = \begin{pmatrix} \lambda & 0 \\ 1 & \lambda \end{pmatrix} = \lambda \begin{pmatrix} 1 & 0 \\ 0 & 1 \end{pmatrix} + \begin{pmatrix} 0 & 0 \\ 1 & 0 \end{pmatrix} \quad (10)$$

[0058] It can be easily shown that a streamline with initial condition $k = (k_1, k_2)$ integrated through such a vector field can be described by:

[0059]
$$x(t) = e^{t\lambda} \cdot \begin{pmatrix} k_1 \\ k_1 t + k_2 \end{pmatrix}$$

[0060] This case resembles an improper node singularity as depicted in **FIG. 4F**.

[0061] *Topological Analysis:* The topological graph (or simply topology) of a vector field describes the structure of the flow or phase portrait. Separatrices are used to separate the areas of the flow into regions with similar behavior. Separatrices can be easily computed by integrating streamlines emerging from saddle singularities in direction of the eigenvalues of the interpolating matrix. The topological graph then consists of the singularities and the separatrices. More complex topological features exist, such as closed streamlines, which can act similarly to singularities due to their attracting or repelling properties

[0062] *Methodology for Extracting Quantitative Information:* The algorithm for determining the curve-skeleton consists of several steps. Since the object is given as a volumetric CT-scanned image, the object boundary must to be extracted first. Then, a vector field is computed that is orthogonal to the object's boundary surface. Once the vector field is computed, the curve-skeleton can be determined by applying a topological analysis to this vector field. In a last

optional step, gaps between segments of the curve-skeleton can be closed automatically. The following subsections explain these steps in detail.

[0063] *Extraction of Object Boundary:* The vasculature that is to be extracted, after the specimen is perfused and CT-scanned, is defined by a volumetric image. A volumetric image consists of voxels aligned along a regular, three-dimensional (3-D) grid. It is generally not likely that the boundary of the vessels is exactly located at these voxels. Hence, better precision can be achieved by finding the exact location in between a set of pixels. Since an accurate representation of the object's boundary is crucial to the algorithm, improving the precision is an essential step. The method used within the described system uses similar techniques as described by Canny's non-maxima suppression but extended to three dimensions.

[0064] First, the image gradients are computed. Using a fixed threshold, all voxels with a gradient length below this threshold are neglected. Then, the gradients of the remaining voxels are compared to its neighbors to identify local maxima along the gradient. In 3-D, the direct neighborhood of a single voxel generally consists of 26 voxels forming a cube that surrounds the current pixel. In order to find the local maximum along the current gradient, the gradients of the neighboring voxels in positive and negative directions have to be determined. When using two-dimensional images, nearest neighbor interpolation of these gradients might work but yield incorrect results in a 3-D volumetric image. Therefore, the gradients on the boundary of the cube formed by the neighboring voxels are interpolated linearly to determine a better approximation of the desired

gradients. **FIG. 5A** explains this in more detail where the current voxel marked as a triangle and its direct neighbors forming a cube are shown. The current gradient is extended to the faces of the cube starting at the current voxel. The resulting intersections, marked as diamonds, define the locations for which the gradients have to be interpolated so that the maximal gradient can be determined. The current implementation of the described system uses linear interpolation.

[0065] Once the neighboring gradients in positive and negative direction of the current gradient are computed, these are compared in order to find local maxima within the data. Thus, if the length of the current gradient is larger than the length of both of its neighbors the local maximum can be calculated just like in the 2-D case. When interpolated quadratically, the three gradients together form a parabolic curve along the direction of the current gradient as shown in **FIG. 5B**. In general, the current gradient is larger than the interpolated neighbors with respect to their lengths since only local maxima were considered in this step. Hence, the local maximum can be identified by determining the zero of the first derivative of the parabolic curve. Determining all local maxima within the volumetric image in this fashion then results in a more accurate and smoother approximation of the object's boundary with sub-voxel precision. Once all points on the boundary are extracted from the volumetric image using this gradient approach with sub-voxel precision, the resulting point cloud can be further processed in order to identify the curve-skeleton.

[0066] *Determination of Vector Field:* The proposed method computes a curve-

skeleton by applying a topological analysis to a vector field that is determined based on the geometric configuration of the object of which the curve-skeleton is to be determined. The vector field is computed in such a way that the vectors are orthogonal to the object's boundary surface. The vectors in between the object are then interpolated linearly.

[0067] Different approaches are possible for calculating such a vector field. A repulsive force field can be determined that uses the surrounding points on the object's boundary surface. The repulsive force is defined similarly to the repulsive force of a generalized potential field. The basic idea is to simulate a potential field that is generated by the force field inside the object by electrically charging the object's boundary. Alternatively, we may define a normal vector by using the neighboring points in addition to the current one and then define a plane that is approximated by these points. The normal of this plane then defines the orthogonal vector corresponding to the current point.

[0068] Since the data is given as a volumetric data set, the image gradients can be used to define the vectors on the object's boundary surface as well. These image gradients are previously determined as they are needed for extracting the object's boundary. Since the points are only moved along the direction of the image gradient when determining the sub-voxel precision, this image gradient is still orthogonal to the object's boundary surface and therefore represents a good approximation for the desired vector field. Note that all three methods result in vectors pointing to the inside of the object.

[0069] *Determination of Curve-Skeleton:* In order to determine the curve-

skeleton of the object, a tetrahedrization of all points on the object's boundary is computed first. For this, Si's very fast implementation of a Delaunay tetrahedrization algorithm is used. By using the previously computed vectors that point to the inside of the vasculature, outside tetrahedra can be distinguished from tetrahedra that are located inside the vessels. This way, all outside tetrahedra can be removed, leaving a Delaunay tetrahedrization of the inside of the vasculature only. Since vectors are known for each vertex of every tetrahedron, the complete vector field can be computed using this tetrahedrization by interpolating tri-linearly within each tetrahedron. This vector field is then used to identify points of the curve-skeleton which are then connected with each other.

[0070] Once the vector field is defined within the entire object, one could use an approach similar to the one used by Cornea et al. and compute the 3-D topological skeleton of the vector field which yields the curve-skeleton of the object. Since singularities are very rare in a 3-D vector field, Cornea et al. had to introduce additional starting points for the separatrices, such as low divergence points and high curvature points, in order to obtain a good representation of the curve-skeleton. Therefore, a different approach is described in this paper that analyzes the vector field on the faces of the tetrahedra.

[0071] In order to perform a topological analysis on the faces of the tetrahedra, the vector field has to be projected onto those faces first. Since tri-linear interpolation is used within the tetrahedra, it is sufficient to project the vectors at the vertices onto each face and then interpolate linearly within the face using

these newly computed vectors. Based on the resulting vector field, a topological analysis can be performed on each face of every tetrahedron.

[0072] Points on the curve-skeleton can then be identified by computing the singularities within the vector field interpolated within each and every face of the tetrahedrization. For example, for a perfectly cylindrical object, the vectors computed at the cylinder's boundary point directly at the center of the cylinder. When looking at the resulting vector field at a cross section of the cylinder, a focus singularity is located at the center of the cylinder within this cross section. The location of this focus singularity resembles a point on the curve-skeleton of the cylinder. Hence, a singularity within a face of a tetrahedron indicates a point of the curve-skeleton. Since the vectors at the object's boundary point inwards, only sinks need to be considered in order to identify the curve-skeleton. Due to the fact that not all objects are cylindrical in shape and due to numerical errors and tolerances, points on the curve-skeleton can be identified by looking for sinks that resemble focus and spiral singularities.

[0073] Obviously, only faces that are close to being a cross section of the object should be considered to identify points on the curve-skeleton. In order to determine tetrahedra whose faces resemble a cross-section of the object, the vectors at the vertices can be used. If the vectors at the vertices, which are orthogonal to the object's boundary, are approximately coplanar with the face, then this face describes a cross section of the object. As a test, the scalar product between the normal vector of the face and the vector at all three vertices can be used. If the result is smaller than a user-defined threshold, this face is

used to determine points on the curve-skeleton. If we compute the singularity on one of these faces, then we obtain a point which is part of the curve-skeleton. Note that since linear interpolation is used within the face, only a single singularity can be present in each face.

[0074] Once individual points of the curve-skeleton are computed by identifying the focus and spiral singularities within the faces of the tetrahedra, this set of points need to be connected in order to retrieve the entire curve-skeleton. Since the tetrahedrization describes the topology of the object, the connectivity information of the tetrahedra can be used. Thus, identified points of the curve-skeleton of neighboring tetrahedra are connected with each other forming the entire curve-skeleton.

[0075] *Closing Gaps within the Curve-Skeleton:* Due to numerical tolerances, sometimes gaps may occur between parts of the curve-skeleton which can be filled automatically. Since the tetrahedrization of the points on the object's boundary describe only the inside of the object, the algorithm can search for loose ends of the curve-skeleton and connect these if they are close to each other. In addition, it is verified that the connection stays within the object; i.e., if it is completely covered by tetrahedra. To test this, those tetrahedra which are close to the line connecting the two candidates and potentially filling a gap are identified. Then, the algorithm computes how much of the line is covered by those tetrahedra; i.e., what fraction of the line is contained within the tetrahedra. If all those fractions add up to 1, then the line is completely within the object and is a valid connection filling a gap of the curve-skeleton.

[0076] *The Algorithm:* The algorithm for extracting curve-skeletons consists basically of several steps. Since the vasculature is given as a volumetric image its boundary needs to be extracted from the volumetric image based on a gradient threshold. To increase accuracy, the points are moved along the gradient direction to achieve sub-pixel precision as previously described. Then, vectors orthogonal to the vascular boundary surface need to be determined. These can be derived from a least-square fit of a plane of a set of neighboring points and then use its normal vector, or the gradient vectors since the vasculature is defined by a volumetric image. Subsequently, the point cloud is tetrahedralized so that the resulting tetrahedra can be used to interpolate the vector field using the previously determined vectors at the vertices. Tetrahedra that are located outside the object are not considered when extracting the curve-skeleton. Finally, the topology can be determined on every face resulting in points on the curve-skeleton. By connecting the points found within two neighboring tetrahedra, the complete curve-skeleton is generated as a last step and the diameters computed as the distance between the centerline and the boundary surface of the vessel.

[0077] The algorithm was tested on a coronary arterial CT image as shown in **FIG. 6**. The proposed algorithm can extract the curve-skeleton from the volumetric data set in order to identify the centerlines of the vessels. The resulting curve-skeleton is depicted in **FIG. 7**. The figure shows the curve-skeleton as well as the point set defining the vascular boundary which was used to find the curve-skeleton. Due to the densely located vessels of the right

coronary arterial (RCA) tree, the extracted curve-skeleton seems rather cluttered and it is difficult to distinguish between lines at different depths. The extracted curve-skeleton, however, exactly describes the centerlines of the arterial vessels found within the data set. When using a sub-section of the porcine coronary image, it can be seen that the curve-skeleton is well defined and located at the center of the arterial vessels, as shown in **FIG. 8**.

[0078] The present invention may be applied to other images and structures in addition to vascular trees. For example, the present method may be used to study the micro-structure of vessel wall (elastin and collagen). Multi-photon microscopy can be used to visualize elastin and collagen fibers separately. The segmentation scheme outlined here can also allow us to reconstruct the fiber structure quantitatively. Many other applications are apparent to one having ordinary skill in the art after consideration of the present disclosure. Such other applications are also within the scope of the present invention.

[0001] The disclosures of all patents, patent applications, and publications cited herein are hereby incorporated herein by reference in their entirety, to the extent that they provide exemplary, procedural, or other details supplementary to those set forth herein. Further, the discussion of a reference in this disclosure is not an admission that it is prior art to the present invention, especially any reference that may have a publication date after the priority date of this application.

[0079] The foregoing disclosure of the exemplary embodiments of the present invention has been presented for purposes of illustration and description. It is not intended to be exhaustive or to limit the invention to the precise forms disclosed.

Many variations and modifications of the embodiments described herein will be apparent to one of ordinary skill in the art in light of the above disclosure. The scope of the invention is to be defined only by the claims appended hereto, and by their equivalents.

[0080] Further, in describing representative embodiments of the present invention, the specification may have presented the method and/or process of the present invention as a particular sequence of steps. However, to the extent that the method or process does not rely on the particular order of steps set forth herein, the method or process should not be limited to the particular sequence of steps described. As one of ordinary skill in the art would appreciate, other sequences of steps may be possible. Therefore, the particular order of the steps set forth in the specification should not be construed as limitations on the claims. In addition, the claims directed to the method and/or process of the present invention should not be limited to the performance of their steps in the order written, and one skilled in the art can readily appreciate that the sequences may be varied and still remain within the spirit and scope of the present invention.

WHAT IS CLAIMED IS:

1. A method to extract morphometric data from a volumetric image; the method comprising the steps of:
 - i. segmenting a plurality of vessels within the volumetric image based on a plurality of image gradients; wherein points resulting from segmentation are moved along the gradient direction in such a way that they are located at the maximal gradient;
 - ii. computing a vector field in such a way that all vectors point inwards to the center of the vessel using a tri-linear interpolation and a tetrahedrization of boundary points; and
 - iii. computing a plurality of points on the centerline of the vessels using a topological analysis of the vector field within the cross sectional area of the vessels; wherein the plurality of points are connected based on the topology of the tetrahedrization.

ABSTRACT

An accurate analysis of the spatial distribution and intravascular pattern of blood flow in any organ must be based on detailed morphometry (diameters, lengths, vessel numbers, branching pattern, branching angles, etc.) of the organ vasculature. Despite the significance of detailed morphometric data, there is relative scarcity of database on vascular anatomy, mainly because the process is extremely labor intensive. Novel methods in the form of a segmentation algorithm for semi-automation of morphometric data extraction are provided. The extraction algorithm is based on a topological analysis of a vector field generated by the normal vectors of the extracted vessel wall. With this approach, special focus is made on achieving the highest accuracy of the measured values, with excellent results when compared to manual measurements of the main trunk of the coronary arteries with microscopy.

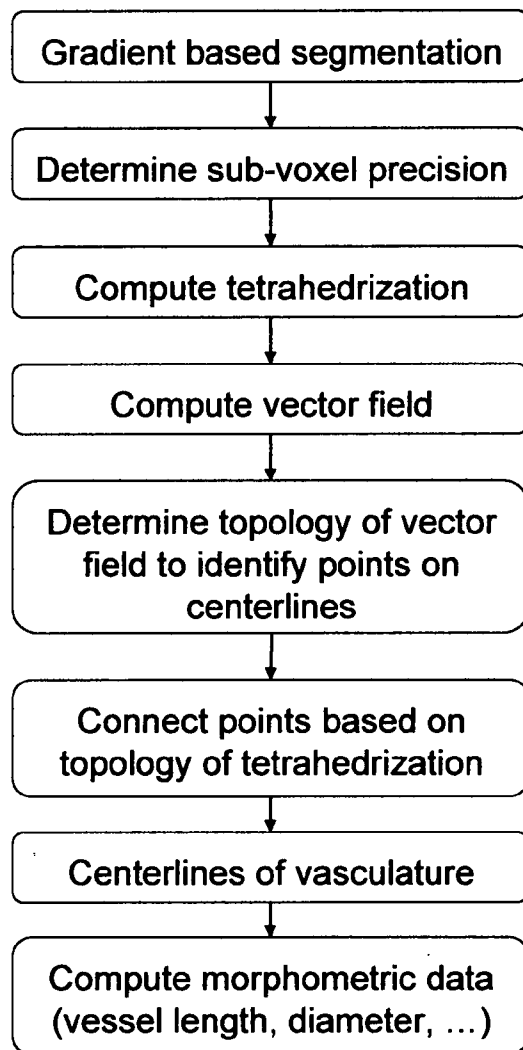
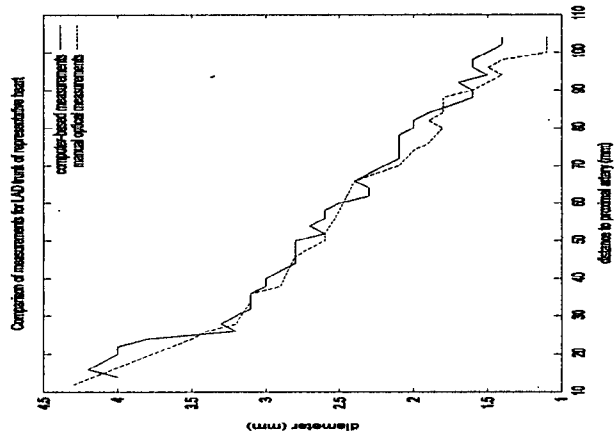
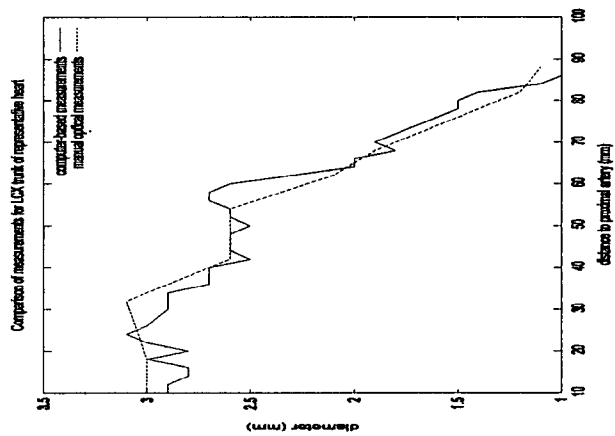


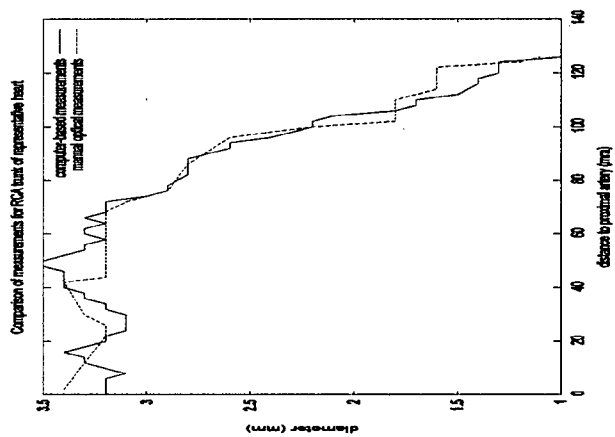
Figure 1



(A)

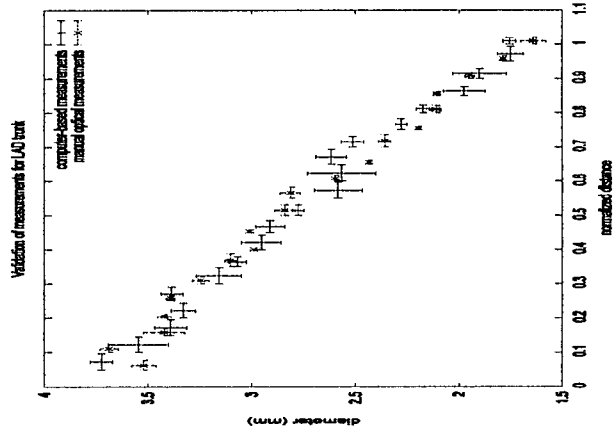


(B)

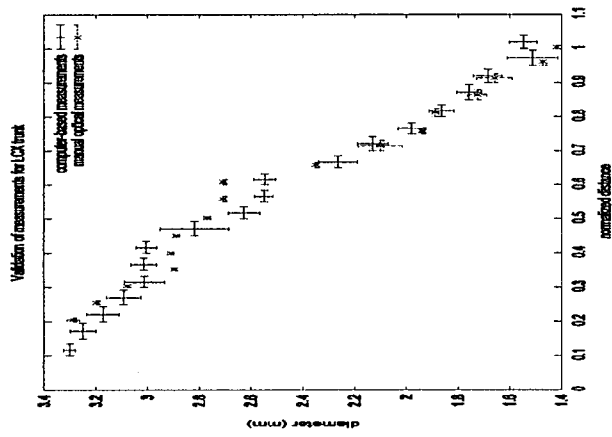


(C)

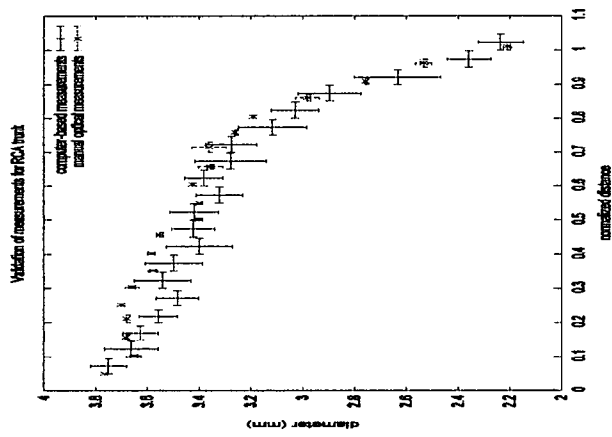
Figure 2



(A)

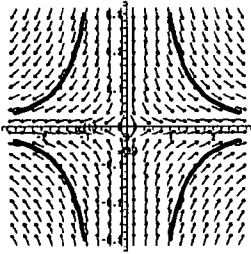


(B)

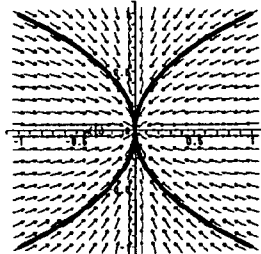


(C)

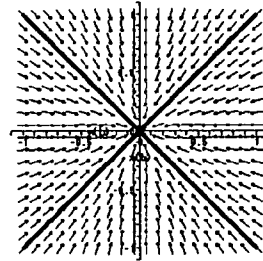
Figure 3



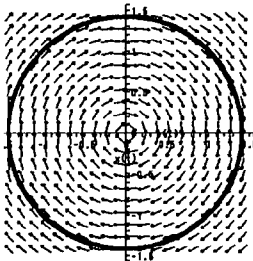
(A)



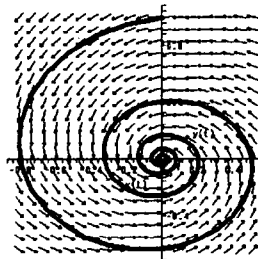
(B)



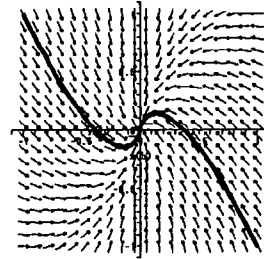
(C)



(D)

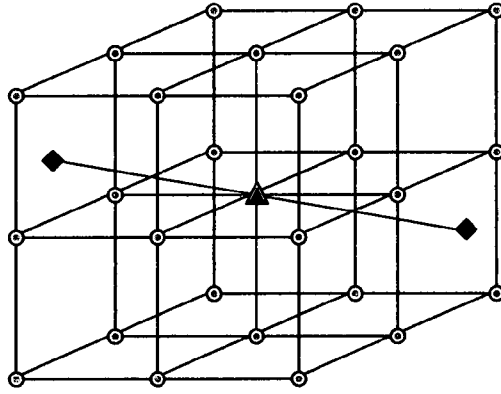


(E)

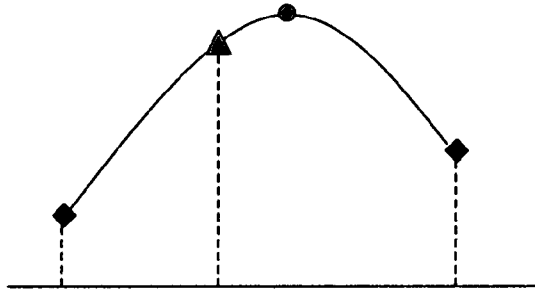


(F)

Figure 4



(A)



(B)

Figure 5

Best Available Copy

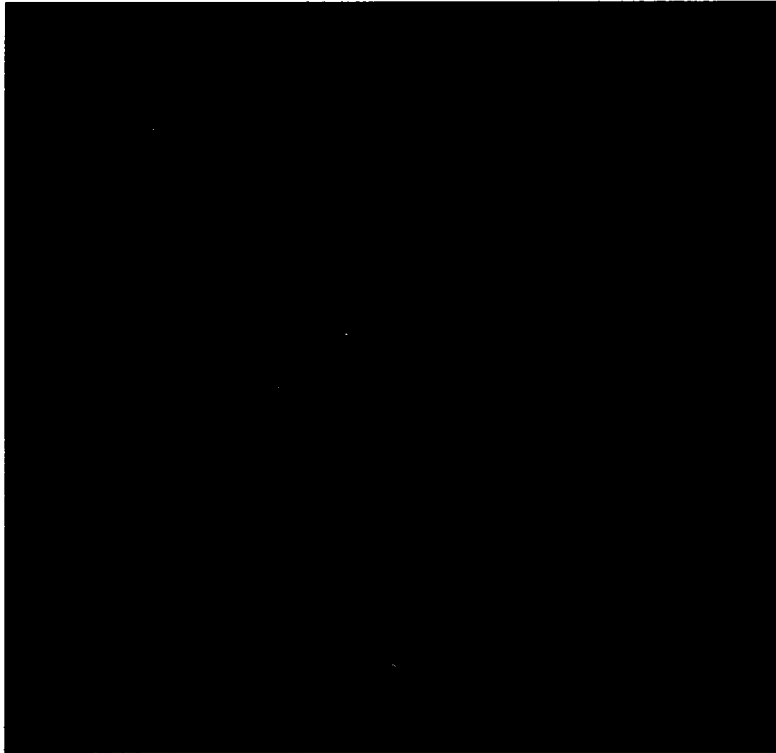
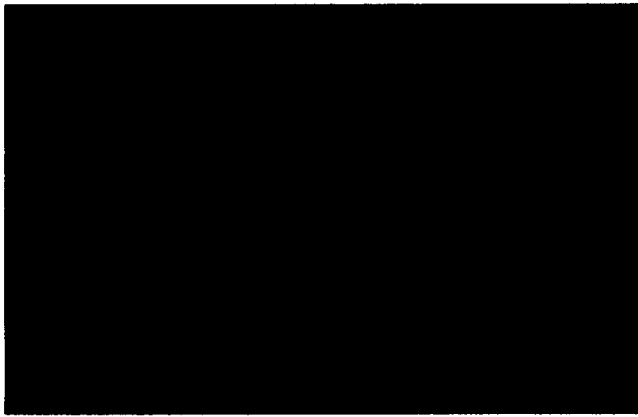


Figure 6

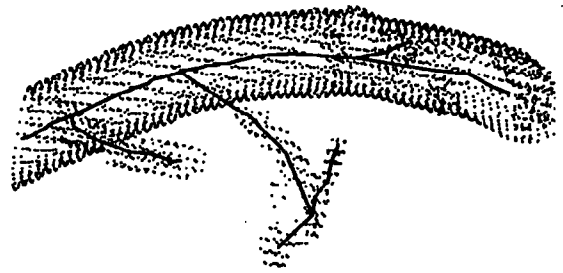


Figure 7

Best Available Copy



(A)



(B)

Figure 8